Noise modelling of wing-in-junction flows

J.L. Coombs (1), C.J. Doolan (1), D.J. Moreau (1), A.C. Zander (1) and L.A. Brooks (2)

(1) School of Mechanical Engineering, University of Adelaide, Adelaide, South Australia, 5005, Australia
(2) ASC Pty Ltd, Osborne, South Australia, 5017, Australia

ABSTRACT

It is important to be able to accurately model the flow and noise generated by wing-in-junction flows because of the many engineering applications in which these flows occur. An incompressible Reynolds-averaged Navier-Stokes (RANS) simulation of a wing-in-junction flow test case was used with a combination of statistical and semi-analytical acoustic models to predict the far-field noise. These noise predictions were compared with experimental measurements taken in an anechoic wind tunnel. The RANS-based noise prediction models were found to achieve good agreement with experimental data.

INTRODUCTION

Wing-in-junction-flows occur where wing-like shapes are attached to a fuselage or hull. The noise generated by wing-in-junction flows impacts on many applications, including aviation where it is a health concern for those that live and work near airfields (Bronzaft et al., 1998, Kaltenbach et al., 2008), as well as electricity-production where the noise inhibits more widespread implementation of wind turbines (Rogers et al., 2006), and in the maritime industry where the reduction of noise for stealth is an especially important consideration for military designs (Defence Science and Technology Organisation, 2004).

The various noise sources in wing-in-junction flows include turbulent boundary layer noise, leading edge noise, turbulent boundary layer trailing edge noise (TBL-TE), and tip noise. To ensure noise modelling can be part of an engineering design process, flow-induced-noise prediction methods must be both accurate and efficient. Hence it is necessary that the most effective noise modelling methods for the radiated sound of wing-in-junction flows be determined to assist those who need to analyse and design devices that incorporate them. This paper aims to extend the RANS-based statistical noise model (RSNM) (Doolan et al., 2010) to three-dimensions, and in combination with a leading edge noise prediction method developed by Amiet (1975), to apply this extension to a wing-in-junction test case, and compare the total predicted noise to experimental anechoic wind tunnel measurements. The finite junction flow test case selected uses a NACA 0012 profile airfoil at Reynolds number based on wing thickness and freestream velocity of $Re_t = 1.932 \times 10^4$.

METHODOLOGY

Amiet-based leading edge noise model

The fluctuating lift experienced by an airfoil leading edge in unsteady flow causes a measure of the flow energy to be radiated as sound to the far-field. A model describing this sound generation process was derived by Amiet (1975). Doolan et al. (2012) proposed an adaptation of the method to incorporate span-wise variations in flow properties and integration with modern computational fluid dynamics codes. This method is used in conjunction with the RSNM trailing edge noise prediction method to predict the total noise of the wing-in-junction flow and compare this prediction to the experimental noise measurements.

RANS-based Statistical Noise Model (RSNM)

Doolan et al. (2010) developed the RANS-based Statistical Noise Model (RSNM) which can be used to predict TBL-TE noise. The method is based on the theory of Ffowcs-Williams and Hall (1970), who use a Green's function approach to calculate the sound intensity in the far field created by turbulent flow past a sharp trailing edge. The Green's function needs to be adapted to the problem geometry, and for a sharp, straight trailing edge, a rigid half plane Green's function is used (Albarracin et al., 2012). The far field pressure fluctuations can be obtained by convolution of the source terms with the Green's function. These source terms could be determined by direct numerical simulation, however, due to the impracticality of such simulation owing to the large computational resources involved, the method models these terms by using the mean flow data from simpler RANS-based simulation by means of a two-point space-time-correlation function model of the form (Morris and Farassat, 2002)

$$R_m(\mathbf{y_1},\boldsymbol{\eta},\tau)=Au_s^2 \exp\left(-\frac{|\boldsymbol{\eta}|^2}{l_s^2}-\omega_s^2\tau^2\right)$$

where $\mathbf{y_1}$ is the position of the first point, $\boldsymbol{\eta}$ the separation between the two points ($\boldsymbol{\eta}=\mathbf{y_2}-\mathbf{y_1}$), A is an empirical scalar value that determines the magnitude of the correlation, l_s the characteristic length scale of the flow, ω_s is a characteristic frequency, u_s is a velocity scale that characterises the velocity fluctuations, and τ the correlation time delay.

Using this two point model the turbulent velocity cross-spectrum becomes in the frequency (ω) domain

$$\Phi(\mathbf{y_1},\boldsymbol{\eta},\omega) = \frac{Au_s^2\sqrt{\pi}}{\omega_s}\exp\left(-\frac{|\boldsymbol{\eta}|^2}{l_s^2}\right)\exp\left(-\frac{\omega^2}{4\omega_s^2}\right)$$

where the model is tied to the RANS turbulence properties by

$$u_s=\sqrt{\frac{2k}{3}},\ \omega_s=\frac{2\pi}{\tau_s},\ \tau_s=\frac{c_\tau k}{\epsilon},\ l_s=\frac{c_l k^{\frac{3}{2}}}{\epsilon}$$

where k and ϵ are the RANS solution turbulent kinetic energy and turbulent dissipation, respectively, and where c_τ and c_l are semi-empirical parameters. For NACA 0012 profile air-

foils such as investigated here, these parameters have been found to take values of A = 1/126, c_τ = 0.11 and c_l = $0.012U_{ref}$ + 0.73, where U_{ref} is the freestream flow velocity (Albarracin et al., 2012).

To date the method has been used successfully on a range of two-dimensional geometry-flow cases including sharp edged flat plates and various airfoils (Doolan et al., 2010, Albarracin et al., 2012); however, it had not been applied to more complex three-dimensional cases and the efficacy of the empirical constants and the assumed form of the turbulent velocity cross-spectrum for such cases is unknown.

3D RSNM methodology

To extend the application of the RSNM method to three-dimensional cases, the following adaptation to the previous detailed turbulent velocity cross-spectrum was proposed:

$$\Phi(\mathbf{y_1},\boldsymbol{\eta},\omega) = \frac{Au_s^2\sqrt{\pi}}{\omega_s}\exp\left(-\frac{|\boldsymbol{\eta_{xy}}|^2}{l_{s_{xy}}^2}\right)\exp\left(-\frac{|\boldsymbol{\eta_z}|^2}{l_{s_z}^2}\right)\exp\left(-\frac{\omega^2}{4\omega_s^2}\right)$$

where the variables are as detailed previously, except that the distance between points ($\boldsymbol{\eta}$), as well as the characteristic length scale of the flow (l_s), have been broken into 2D-equivalent and spanwise components labelled with the subscripts xy and z, respectively. Such a form allows for differing correlation strengths to be applied to the 2D-equivalent and spanwise directions, and it is expected that future work will involve determining whether these parameters are dependant on the airfoil geometry and/or Reynolds number. However, for the present study, the spanwise coefficients will take the same values as their 2D equivalents, to see how well the method performs without tuning of the constants for this specific case.

In order to use the CFD results for the sound calculations, all of the RANS model cell volumes and cell centre positions were calculated. Along with the cell centred values for velocity and turbulence properties, these were passed into the sound prediction code, and thus the sound calculation was performed on the same volumes as the CFD.

Geometry and boundary conditions

The geometry is a finite NACA 0012 wing attached at zero angle of attack to a flat plate wall as shown in Figure 1. The Cartesian coordinate system, with origin at the wing-plate interface, is also shown. The wing chord (C) and span (S) are both 69 mm.

The four boundaries on this domain are the solid surface formed by the wing-plate, the outlet which consists of the *Y-Z* plane at *X*=15C as well as the *X-Z* planes at *Y*=±2.5C, the top *X-Z* plane at *Z*=10C, and the inlet at *X*=-6.845C in the *Y-Z* plane.

The top plane had a slip boundary condition applied to it while the wing-plate pair was given a no-slip condition. The condition applied on the outlet was a zero-gradient condition. The inlet had a uniform velocity of 35 m/s, with turbulence properties estimated using the eddy viscosity ratio method with an assumed eddy viscosity ratio of unity and turbulence intensity set to 0.3%, matching the intensity of the wind tunnel facility, resulting in values of turbulent kinetic energy, k = 0.0165375 m^2s^{-2}, and dissipation, ε = 1.641 m^2s^{-3}, for the inlet. The Reynolds stress tensor terms were derived from the velocity field using the OpenFOAM™ (Weller et al., 1998) Reynolds shear stress tool. Experimentally the boundary layer height on the flat plate in absence of the airfoil was measured as δ = 9.7 mm at a distance 60 mm upstream of the location equivalent to the position of the leading edge of the airfoil. The inlet position for the simulation was set so that uniform inlet boundary conditions would develop a flat plate boundary layer with height matching this experimental measurement, based on the flat plate turbulent boundary layer power law equation,

$$\frac{\delta}{\mathbf{x}} \cong 0.37{R_x}^{-0.2},$$

where δ is the boundary layer height, **x** the flat plate distance, and R_x the Reynolds number based on the flat plate distance. When this is solved for the measured 9.7 mm boundary layer height and added to the 60 mm that the measurement was taken upstream of the airfoil location, a total upstream distance of 0.4723 m (6.845 C) is determined to be required in order to match the experimental and simulation boundary layer heights.

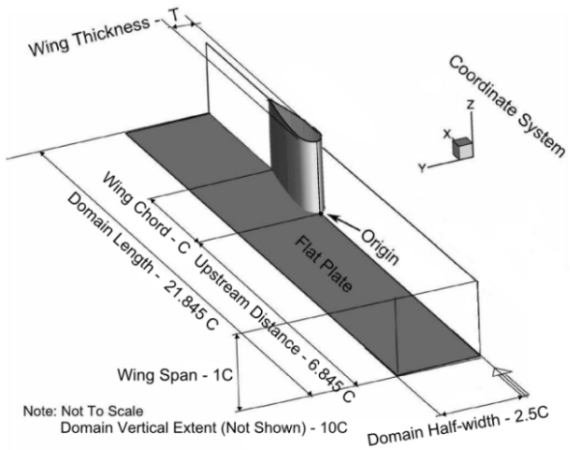

Figure 1. Geometry and coordinate system (adapted from Paciorri et al., 2005)

RANS details, meshing and numerical methods

The flow was treated as incompressible and solved using the OpenFOAM™ code using the Semi-Implicit Method for Pressure-Linked Equations algorithm. The RANS equations were solved using the Launder Reece Rodi (Launder et al., 1975) model for closure due to its effectiveness for wing-in-junction flows (Coombs et al., 2012).

Linear interpolation schemes were used throughout, as was a second-order accurate linear scheme for the discretisation of gradient terms. The divergence terms were discretised using a first-order accurate upwind scheme. All Laplacian terms were discretised with the second-order accurate linear scheme with explicit non-orthogonal correction. Finally, explicit non-orthogonal correction was performed when calculating surface-normal gradient terms.

The mesh had 1.9×10^6 cells and the solution had a wing average non-dimensional wall distance y^+ (Wilcox, 2006) of 26.86. The solution was run until all residuals reached a level of 10^{-5} or smaller. Wall functions for the turbulent viscosity and dissipation were used throughout.

Experimental method

The experiment was performed in the anechoic wind tunnel at the University of Adelaide. The test chamber of the anech-

oic wind tunnel is 1.4 x 1.4 x 1.6 m (internal dimension) and the facility contains a rectangular flow contraction that has dimensions of 75 mm x 275 mm (Moreau et al., 2011).

Testing was conducted on a finite length NACA 0012 airfoil mounted on a flat plate at equivalent conditions to those in the numerical simulations. In the experiment, the airfoil was tripped at 10% chord using a 12 mm wide serrated strip of double sided tape covered in fine sand. Acoustic data were recorded at a single observation location using a B&K 1/2" microphone (Model No. 4190) located at (x,y,z) = (34.5,500,69) mm, a distance y=500 mm above a point at the middle of the chord at the free end of the airfoil. Additionally, hot-wire anemometry (using a TSI 1210-T1.5 single-wire probe) was used to measure velocity profiles in the near trailing edge wake. Acoustic and velocity data was recorded using a National Instruments PCI-4472 board at a sampling frequency of 5×10^4 Hz with sample durations of 30 seconds and 20 seconds, respectively. Vertical velocity profiles consist of data measured at 141 locations with a spacing of 0.1 mm, while spanwise velocity profiles consist of data measured at 154 locations with a spacing of 0.5 mm. Further details of the methodology are described in Moreau et al. (2013).

RESULTS AND DISCUSSION

CFD results and comparison

Figure 2 shows the location of the planes and lines at which comparisons will be made between the experimental and CFD results. Velocity ($U_{mag} = |u|$), as well as turbulent kinetic energy (k) will be compared. The spanwise samples are taken in the chordwise symmetry plane 1 mm downstream of the TE. The samples taken at plate normal distances (z) of 39, 64 and 69 mm, are also taken 1mm downstream of the TE.

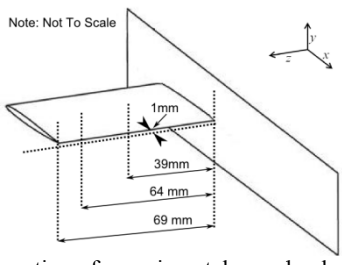

Figure 2. Location of experimental sample planes of interest

The flow profiles at 39, 64 and 69 mm shown in Figures 3 to 5 are significantly more symmetric than those from the experiment, especially the 64 mm line profile, in which the simulation velocity profiles can be seen to closely agree with the experimental values on one side of the airfoil but not on the other. The broken symmetry of the experimental data could in part be attributed to inexact angle of attack positioning of the model, as well as positional error during experimental sampling.

The simulated symmetry line velocity profile shown in Figure 6, somewhat underpredicts the experimentally measured velocity levels in the mid region, but is in good agreement at the root and tip.

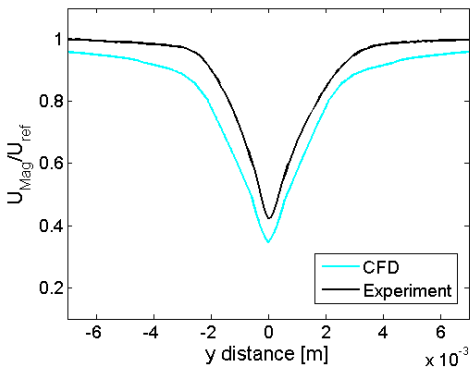

Figure 3. z = 39 mm plate-normal velocity comparison

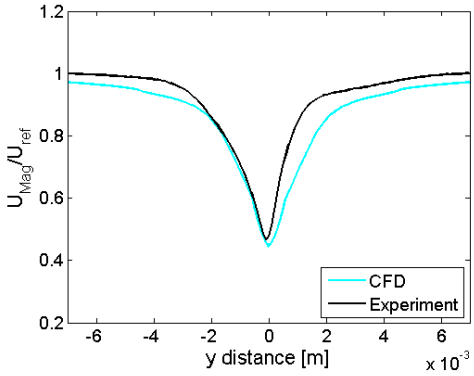

Figure 4. z = 64 mm plate-normal velocity comparison

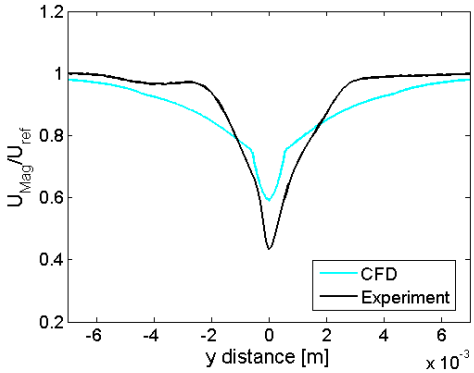

Figure 5. z = 69 mm plate-normal velocity comparison

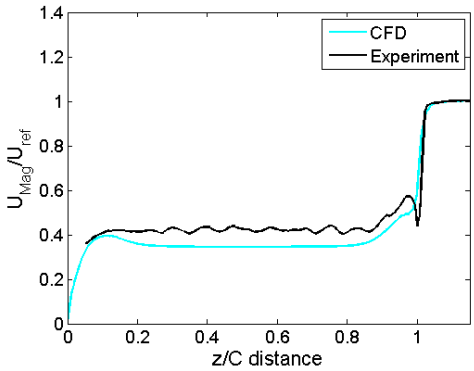

Figure 6. Spanwise symmetry line velocity comparison

The flow profiles at 39, 64 and 69 mm shown in Figures 7 to 9 show that the CFD tends to correctly predict the intensity of the turbulence profiles, but does not resolve the finely detailed profile shapes, as seen in the experimental 69 mm profile shown in Figure 9. This is due to the size of the cells

which was limited by the need for tractable CFD mesh cell expansion ratios during meshing and also the need to satisfy the y^+ limits required by the wall functions used. It is expected that such detail could be captured by abandoning a wall function approach and instead using a much finer mesh and an appropriate low-Re formulated RANS model. It should be noted that the experimental measurements only measured two velocity components, and for comparison to the simulation the third component was estimated assuming a 4:2:3 ratio between u`:v`:w`, which is known to hold for flat plate boundary layers (Wilcox, 2006), and the 'corrected experiment' profiles shown in Figures 7 to 9 incorporate this component. Except for the mean velocity profile at the tip of the airfoil, the simulated and experimentally measured flow results have shown good agreement throughout.

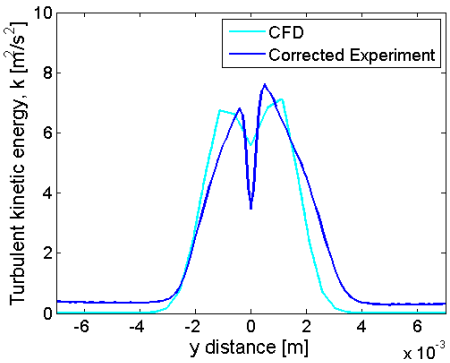

Figure 7. z = 39 mm plate-normal turbulent kinetic energy comparison

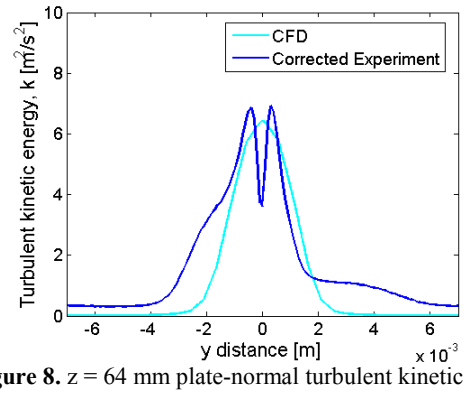

Figure 8. z = 64 mm plate-normal turbulent kinetic energy comparison

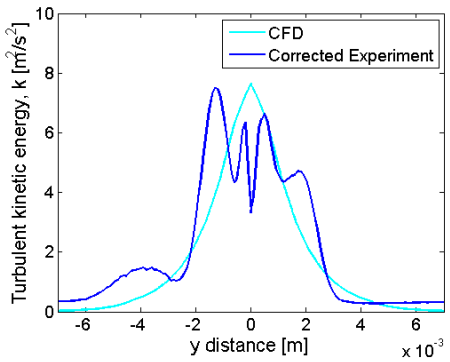

Figure 9. z = 69 mm plate-normal turbulent kinetic energy comparison

Sound prediction results

Work to date using the RSNM method has shown that if too small a sample region is used, it adversely affects the results, and that generally, a region that extends one boundary layer height upstream, downstream and across-stream of the TE is sufficient to achieve a sample size independent solution (Doolan et al., 2010). To check that a sufficiently large sample region was used, three sample volumes of increasing extent were defined, and the predictions using each of the sample volumes compared. The small sample volume had extent $(\Delta x,\Delta y,\Delta z) = (2\delta,\delta,S)$, while the medium and large sample volumes had extents of $(\Delta x,\Delta y,\Delta z) = (4\delta,2\delta,S)$ and $(\Delta x,\Delta y,\Delta z) = (6\delta,3\delta,S)$ respectively, and all volumes had centres coinciding with the mid-span of the TE of the airfoil at (x,y,z) = (0.069,0,0.0345) mm. Predictions achieved using these sample volumes are compared in Figure 10. Little dependence was found on the size of the volume region, with the results between the medium and large sample volumes differing by less than 0.5 dB across the 250 Hz – 10 kHz one-third octave bands.

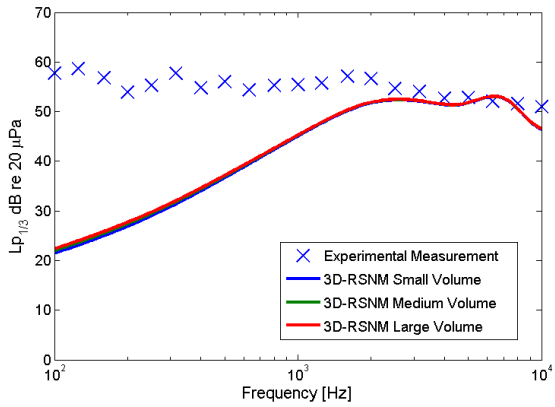

Figure 10. 3D RSNM sample region independence

The CFD data used for the leading edge sound prediction model was obtained at a location one quarter chord upstream of the leading edge to ensure the flow was unaffected by the wing and was similar to the flow entering the computational domain. Figure 11 gives the predictions of both the leading and trailing edge noise predictions. It is seen that the leading edge component dominates at low frequencies (<1 kHz) while the trailing edge component dominates at high frequencies (>2 kHz), and that there is good agreement between the predicted and measured levels. It would seem therefore that for the frequency ranges considered that the leading edge and trailing edge noise components account for the majority of the noise. It is believed that the 3D-RSNM method will prove adaptable to calculating the tip noise component. Undertaking this adaption, as well as predicting the tip noise component for this test case, are identified as areas of future work.

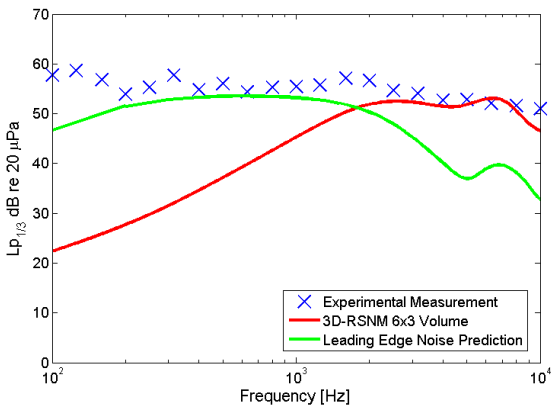

Figure 11. Modelled noise predictions and experimental measurement

CONCLUSIONS

Results of a study of flow and noise modelling of a wing-in-junction flow have been presented. A CFD simulation was performed, and comparisons made between the simulated and experimental flow results. The CFD results were then used in conjunction with statistical and semi-analytical noise prediction methods, the results of which were compared to experimental noise measurements. The leading edge noise component was seen to dominate at low frequency while the trailing edge component was seen to dominate at high frequency. When combined, these noise components predicted the total noise well. Future work on the 3D-RSNM model was identified and is expected to include determining how, if at all, the spanwise coefficient constants should differ from the traditional values, as well as its adaptation to compute tip noise.

Acknowledgments

This work has been supported by the Australian Research Council under Linkage grant LP110100033 'Understanding and predicting submarine hydrofoil noise'.

References

Albarracin, C, Doolan, C, Jones, R, Hansen, C, Brooks, L & Teubner, M 2012, 'A RANS-based Statistical Noise Model for Trailing Edge Noise', *AIAA 18th AIAA/CEAS Aeroacoustics Conference*, Colorado Springs, USA.

Amiet, R 1975, 'Acoustic radiation from an airfoil in a turbulent stream', *Journal of Sound and Vibration,* vol. 41, pp. 407-420.

Bronzaft, A, Ahern, K, McGinn, R, O'Connor, J & Savino, B 1998, 'Aircraft noise: A potential health hazard.' *Environment and Behavior*, volume 30, pp. 101-113.

Coombs, J, Doolan, C, Moreau, D, Zander, A & Brooks, L 2012, 'Assessment of turbulence models for a wing-in-junction flow', *18th Australasian Fluid Mechanics Conference Launceston*, Launceston, Australia.

Defence Science and Technology Organisation 2004, 'Some aspects of submarine design part 1. Hydrodynamics', Technical report.

Doolan, C, Coombs, C, Moreau, D, Zander, A & Brooks, L 2012, 'Prediction of noise from a wing-in-junction flow using computational fluid dynamics', *Australian Acoustical Society Proceedings of Acoustics 2012*, Fremantle, Australia.

Doolan, C, Gonzalez, C & Hansen, C 2010, 'Statistical estimation of turbulent trailing edge noise.', *Proceedings of 20th International Congress on Acoustics*, ICA 2010.

Ffowcs-Williams, J & Hall, L 1970, 'Aerodynamic sound generation by turbulent flow in the vicinity of a scattering half plane', *Journal of Fluid Mechanics* , vol. 40, pp. 657-670.

Kaltenbach, M, Maschke, C & Klinke, R 2008, 'Health consequences of aircraft noise.' *Deutsches Arzteblatt International*, volume 105, pp. 548–556.

Launder, B, Reece, G & Rodi, W 1975, 'Progress in the development of a Reynolds-stress turbulence closure', *Journal of Fluid Mechanics*, vol. 68, no. 3, pp. 537-566.

Moreau, D, Brooks, L & Doolan, C 2011, 'Broadband trailing edge noise from a sharp-edged strut', *Journal of the Acoustical Society of America*, vol. 129, no. 5, pp. 2820-2829.

Moreau, D & Doolan, C 2013, 'An experimental study of the sound produced by junction flows', *Proceedings of the 20th International Congress on Sound and Vibration*, Bangkok, Thailand, paper no. 18.

Morris, P & Farassat, F 2002, 'Acoustic Analogy and Alternative Theories for Jet Noise Prediction', AIAA Journal, vol. 40, no. 5, pp. 671-680.

Paciorri, R, Figlioli, A, Mascio, AD & Favini, B 2005, 'RANS simulations of a junction flow', *International Journal of Computational Fluid Dynamics*, vol 19, no. 2, pp. 179-189.

Rogers, A, Manwell, J & Wright, S 2006, 'Wind turbine acoustic noise', Renewable Energy Research Laboratory, University of Massachusetts at Amherst.

Weller, H, Tabor, G, Jasak, H & Fureby, C 1998, 'A tensorial approach to CFD using object orientated techniques'. *Computers in Physics*, vol. 12, pp. 620-631.

Wilcox, D 2006, *Turbulence Modeling for CFD*, DCW Industries Inc., California, USA.